Optical and structural properties of Al 2 O 3 doped ZnO nanotubes prepared by ALD and their photocatalytic application

Maryline Nasr, Roman Viter, Cynthia Eid, Roland Habchi, Philippe Miele, Mikhael Bechelany

Optical and structural properties of Al_2O_3 doped ZnO nanotubes prepared by ALD and their photocatalytic application

Maryline Nasr,[1,2] Roman Viter,*[3] Cynthia Eid,[2] Roland Habchi,[2] Philippe Miele[1,4] and Mikhael Bechelany*[1]

[1]Institut Européen des Membranes IEM, UMR-5635, Université de Montpellier, ENSCM, CNRS, Place Eugène Bataillon, F-34095 Montpellier Cedex 5, France

[2]EC2M, Faculty of Sciences 2, campus Pierre Gemayel, Fanar, Lebanese University, 90656 Lebanon

[3] Institute of Atomic Physics and Spectroscopy, University of Latvia, 19 Raina Blvd., LV 1586 Riga, Latvia

[4]Institut Universitaire de France (IUF)

* Corresponding authors: mikhael.bechelany@umontpellier.fr,

Phone: +33467149167, Fax: +33467149119

viter_r@mail.ru, Phone: +371 20 058 754

Abstract

Al_2O_3 doped ZnO nanotubes with controlled ratio of Al_2O_3 were successfully designed by combining the two techniques of atomic layer deposition (ALD) and electrospinnig. In order to study the effect of Al_2O_3 doping on optical and structural properties of Al_2O_3 doped ZnO nanotubes, the prepared samples were analyzed by scanning electron microscopy (SEM), X-

ray diffraction (XRD), energy-dispersive X-ray spectroscopy (EDX), Fourier-transform infrared (FTIR), reflectance emission and room temperature photoluminescence (PL). The photocatalytic activity and stability of these materials under UV light was studied by the photodegradation of methyl orange (MO). The results indicate that Al_2O_3 doping increases the disorder (defects and oxygen vacancies formation) in the ZnO nanostructure which improves the separation efficiency of electron-hole pairs and therefore enhances the photocatalytic activity (5 times higher) and stability of Al_2O_3 doped ZnO in comparison with pure ZnO nanotubes.

TOC Graphic

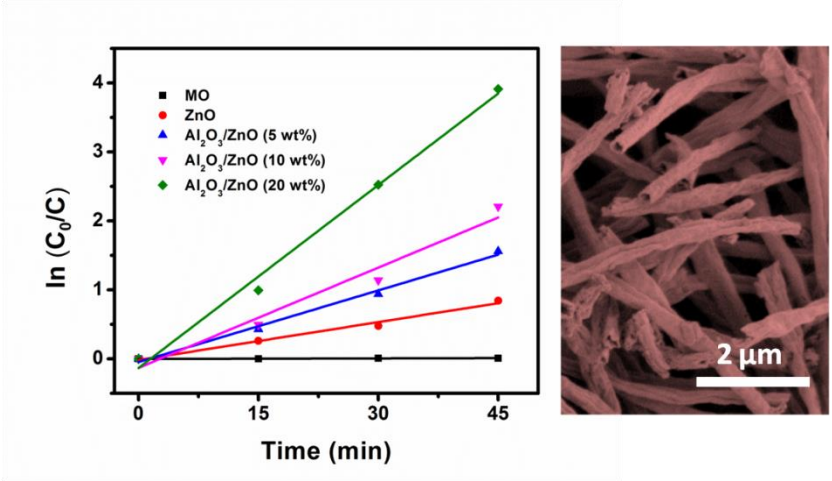

1. Introduction

The green technology, “photocatalysis”, is one of the less expensive and more efficient methods for wastewater treatment. In recent years, the attention of the researchers has been given to the semiconducting oxide photocatalysts due to their potential applications in solar energy conversion[1] and environmental purification.[2] Zinc oxide (ZnO) with a wide band gap (3.3 eV) is one of the most effective photocatalysts under UV light due to its high activity, low cost and environmental safety.[3] However, the fast electron-hole pairs’

recombination in ZnO limits the high efficiency of the photocatalytic reaction.[4] In previous studies, many efforts have been developed to improve the separation efficiency of the photogenerated pairs, including doping ZnO with other oxides (In_2O_3, SnO_2, NiO …).[5-7] It is well known that doping ZnO with Aluminum oxide (Al_2O_3) improves its optical and structural properties which will influence its photocatalytic activity.[8] Therefore, in order to study the effect of the optical properties on the photocatalytic activity, Al_2O_3 doped ZnO nanotubes were synthesized by combining the two techniques of Atomic Layer Deposition (ALD) and Electrospinning. ALD is a unique and powerful vapor-phase deposition technique to fabricate different oxides materials. The ALD technique ensures a precise thickness control, chemical composition, high quality conformal and homogenous deposited layers.[9] Electropsinning is a simple and cost effective technique that took much attention because of its capability in generating large amounts of nanofibers with the use of high electrical field.[10] In the present work, as a first step, PAN nanofibers were synthesized by electrospinning technique.[11] The second step is metal oxides deposition by ALD.[12] After the heat treatment, the prepared samples were characterized in order to study their structural, morphological and optical properties. The photodegradation of methyl orange under UV was investigated to study the photocatalytic activity and stability of the ZnO and Al_2O_3/ZnO nanotubes.

2. Experimental section

2.1. Chemicals and materials

Diethyl zinc {(DEZ), Zn $(CH_2CH_3)_2$, 95%} and trimethylaluminum {(TMA), Al $(CH_3)_3$, 97%} were used as precursors for ZnO and Al_2O_3 respectively. N,N-dimethylformamide (DMF; 99.8%) and polyacrylonitrile (PAN; MW = 500 000) were used to elaborate PAN nanofibers. Methyl orange (MO) was used as a pollutant to evaluate the photocatalytic

activity of the samples. All chemicals were purchased from Sigma Aldrich and used without any further purification.

2.2. Preparation of PAN nanofibers

The electrospinning process was used to synthesize PAN nanofibers. The polymer solution was prepared by dissolving 10 wt% of polyacrylonitrile in dimethylformamide. The mixture was maintained under agitation for 4 hours and then was loaded into a plastic syringe having a stainless steel needle with a diameter of 0.7 mm. The electrospinning process was performed at 38 ± 5°C with an applied voltage of 25 kV. The flow rate was fixed at 1 $ml.h^{-1}$ and the distance between the tip of the needle and the aluminum foil was maintained at 20 cm. Nanofibers were collected on a rotating coil covered with an aluminum foil with a rotation speed of 400 rpm.

2.3. ALD sequences

A homemade ALD reactor was used for the synthesis of ZnO and AL_2O_3/ZnO nanotubes. All the ALD depositions were performed at 60°C using the following sequence mentioned in Table 1. The precursor pulses were coupled with 25 sccm Ar flow as a gas vector; purge was performed with 100 sccm Ar flow as a gas vector. PAN nanofibers were heated at 500°C after the ALD deposition with a heating rate of $1°C.min^{-1}$ for 8 hours in air to eliminate the core of carbon in order to obtain ZnO and Al_2O_3/ZnO nanotubes. As shown in Table 2, Al_2O_3 doped ZnO nanotubes with different ratios of Zn/Al were obtained by alternating the deposition sequences of Al_2O_3 and ZnO cycles on the PAN nanofibers.

Table 1. Step time investigation of Al_2O_3 and ZnO deposition on PAN nanofibers.

	Pulse	**Exposure**	**Purge**	**Water Pulse**	**Exposure**	**Purge**
Time	**Al_2O_3 (TMA)**					

	0.2s	30s	40s	2s	30s	40s
	ZnO (DEZ)					
	0.4s	20s	40s	2s	30s	40s

Table 2. Deposition sequences of Al_2O_3 and ZnO cycles on the PAN nanofibers

Samples	**Deposition sequences**		
	ZnO cycle	**Al_2O_3 cycle**	**Repetition**
ZnO	1	0	100
Al_2O_3/ZnO (5 wt%)	20	1	5
Al_2O_3/ZnO (10 wt%)	10	1	10
Al_2O_3/ZnO (20 wt%)	5	1	20

2.4. Chemical and structural characterization

Scanning electron microscopy (SEM) images were taken with a Hitachi S4800, Japan. Energy-dispersive X-ray spectroscopy analyses (EDX) were taken with a Zeiss EVO HD15 microscope coupled with an Oxford X-MaxN EDX detector. X-ray diffraction (XRD) measurements were carried out using a PANAlytical Xpert-PRO diffractometer equipped with an X'celerator detector using Ni-filtered Cu-radiation (λ= 1.54 ˚A). Optical properties were analyzed by diffuse reflectance (Shimadzu UV-3600). Photoluminescence (PL) spectra of Al_2O_3/ZnO nanotubes were measured in the range of 350-850 nm using HR2000+ Ocean

Optics spectrometer (USA). Excitation of photoluminescence was performed by nitrogen laser LGI (Russia) (λ=337 nm, output power 2.5 mW, 100 Hz).

2.5. Measurement of photocatalytic activity

The photocatalytic activity of ZnO and Al_2O_3 doped ZnO nanotubes was evaluated by the degradation of methyl orange (MO) solution under UV light irradiation (obtained from a 400 W light source, emission wavelength < 380 nm). The reaction temperature was kept constant at 25 ± 2°C by circulating water in a cylindrical tube surrounding the photo-reactor during the entire experiment. MO was used as a reference for organic pollutants. The decomposition was carried out in several beakers containing a suspension of 10 mg from each photocatalyst and 25 mL of MO solution (20 $mg.L^{-1}$). Prior to light irradiation, the suspension was stirred for 1 h in the dark to obtain a good dispersion and to reach the adsorption-desorption equilibrium. Then, the solution was irradiated with UV light for 45 minutes. The distance between the lamp and the dye solution was maintained at 10 cm. Every 15 min, 3 ml of the sample solution was taken out and centrifuged to remove the catalyst. The centrifuged solutions were analyzed by a UV-VIS spectrometer in order to evaluate the decrease in the dye concentration. After irradiation, the photocatalytic degradation efficiency percentage has been calculated as follow:[13]

$$\text{Degradation efficiency (\%)} = (C_0 - C)/C_0 \times 100 \qquad \text{(Equation 1)}$$

Where C_0 is the initial concentration and C is the final concentration of dye before and after photo-irradiation respectively. The mechanism of the photodegradation of MO by a semiconductor (SC) is proposed as follows [14]:

$$SC + hv \rightarrow SC\,(h^+, e^-) \qquad \text{(Equation 2)}$$

$$h^+_{\text{(valence band)}} + OH^- \rightarrow HO^{\bullet} \qquad \text{(Equation 3)}$$

$$e^-_{\text{(conduction band)}} + O_2 \rightarrow O_2^- \qquad \text{(Equation 4)}$$

$$MO + HO^{\bullet} \text{ or } O_2^- \rightarrow \text{Degraded products} \qquad \text{(Equation 5)}$$

The absorption of a photon by the semiconductor ($hv \geq E_g$) will cause an excitation of an electron from its valence band to its conduction band creating a positively charged hole (h^+) in the valence band. Thus, the hole can migrate to the surface of the semiconductor react with adsorbed OH^- to produce hydroxyl radicals ($HO^{\bullet}$), whereas the electrons from the conduction band migrate to the surface and react with adsorbed electron acceptors, such as O_2 in order to degrade the pollutant (MO) (Equation 2 to 5).

3. Results and discussion

3.1. Morphological and Structural properties of ZnO and Al_2O_3/ZnO nanotubes

The nanotubes of ZnO and Al_2O_3 doped ZnO were elaborated by combining the two techniques: Electrospinning and ALD. After the heat treatment, the morphological properties of the as-prepared samples were analyzed by scanning electron microscopy. The SEM images in figure 1 show the well-defined nanotubes morphology of ZnO, Al_2O_3/ZnO (5 wt%), Al_2O_3/ZnO (10 wt%) and Al_2O_3/ZnO (20 wt%). The average diameter was measured on 100 randomly chosen nanotubes of each sample. The diameters were measured from the SEM images using image analysis software (Image J1.29X). No significant changes were detected in the average diameter of the prepared nanotubes; the obtained value was 300 ± 20 nm for all samples. EDX data of ZnO and Al_2O_3/ZnO nanotubes reported in table 3 show the presence of the three elements Zn, Al and O without detection of any impurities. In addition, the increase of the atomic percentage of Al with the doping amount of Al_2O_3 can be clearly seen from table 3.

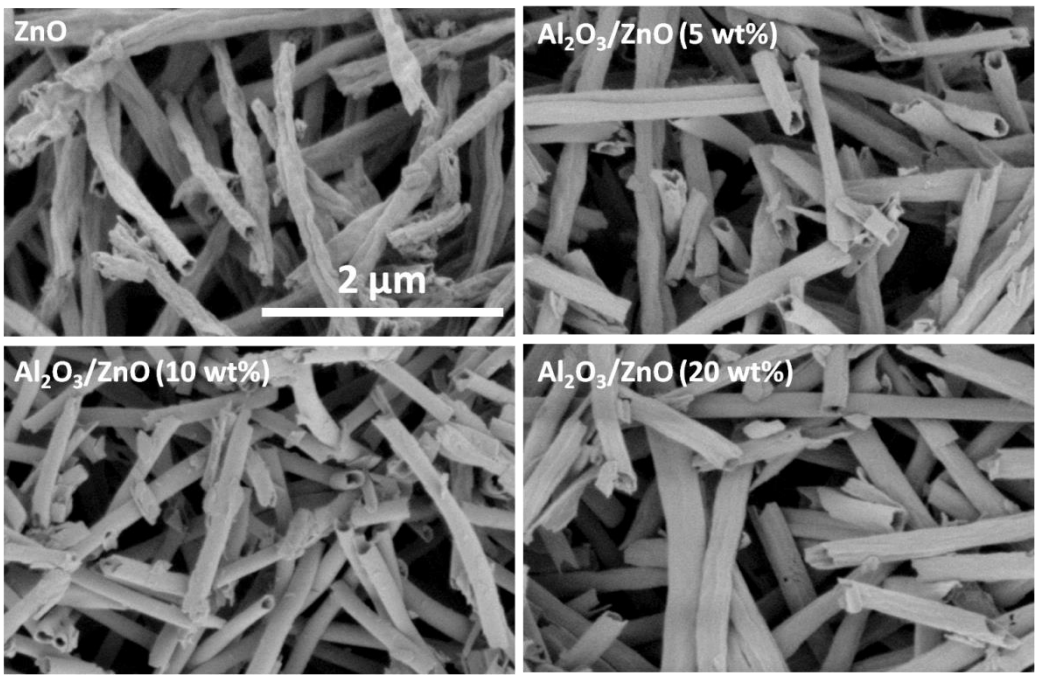

Figure 1. Scanning Electron Microscope images of ZnO and Al_2O_3 doped ZnO annealed nanotubes in air for 8h at 500°C.

Table 3. EDX data showing the atomic percentage composition of ZnO and Al_2O_3/ZnO prepared samples.

	Atomic percentage (±1%)		
Samples	**Zn**	**Al**	**O**
ZnO	48	-	52
Al_2O_3/ZnO (5 wt%)	49	4	47
Al_2O_3/ZnO (10 wt%)	37	8	55
Al_2O_3/ZnO (20 wt%)	36	14	50

The XRD patterns of the prepared samples presented in Figure 2 show the diffraction peaks of the hexagonal wurtzite crystalline phase of zinc oxide (100), (002), (101), (102), (110), (103), (200), (112) and (201) corresponding to 2θ = 31.7, 34.4, 36.2, 47.5, 56.5, 62.8, 66.3, 67.9 and 69.0, respectively.[15] The peak shift towards higher values of 2θ and the peak widening were observed with the increase of Al_2O_3 concentration. Lattice constants (a and c), and interplane distances (d) were calculated from XRD data (Table 4). The increase of Al_2O_3 concentration results in a decrease of the lattice constants and interplane distances. The mechanism of these structural changes is related to the substitution of Zn^{2+} ions with Al^{3+} ions. As the radius of Al^{3+} ion (0.053 nm) is much lower than the radius of Zn^{2+} ion (0.074 nm), a decrease of lattice constants is expected with an increase of Al_2O_3 dopant concentration.[16] The average grain size D (nm) was calculated using Debye-Scherrer equation:[17]

$$D = k\lambda/\beta\cos\theta \qquad \text{(Equation 6)}$$

where k is the shape factor constant (0.9), λ is the X-ray wavelength (0.154 nm), β is the line broadening of the diffraction line measured by the full width at half maximum of the peak intensity (FWHM) and θ is the Bragg angle (in degrees).The obtained grain size values were 16 nm, 10 nm, 9 nm and 9 nm for ZnO, Al_2O_3/ZnO (5 wt%), Al_2O_3/ZnO (10 wt%) and Al_2O_3/ZnO (20 wt%), respectively. The decrease of the crystalline structure of ZnO with Al_2O_3 doping amount is due to the amorphous state of Al_2O_3. Thus, the growth of ZnO crystals is stopped by the amorphous Al_2O_3 layers.[8] Strain values (ε) were calculated due to the following equation:

$$\varepsilon = \beta/4\tan(\theta) \qquad \text{(Equation 7)}$$

where θ and β are diffraction angle and full width of half maximum, respectively. The obtained strain values were 0.0068, 0.01, 0.011 and 0.012 for ZnO, Al_2O_3/ZnO (5 wt%), Al_2O_3/ZnO (10 wt%) and Al_2O_3/ZnO (20 wt%), respectively.

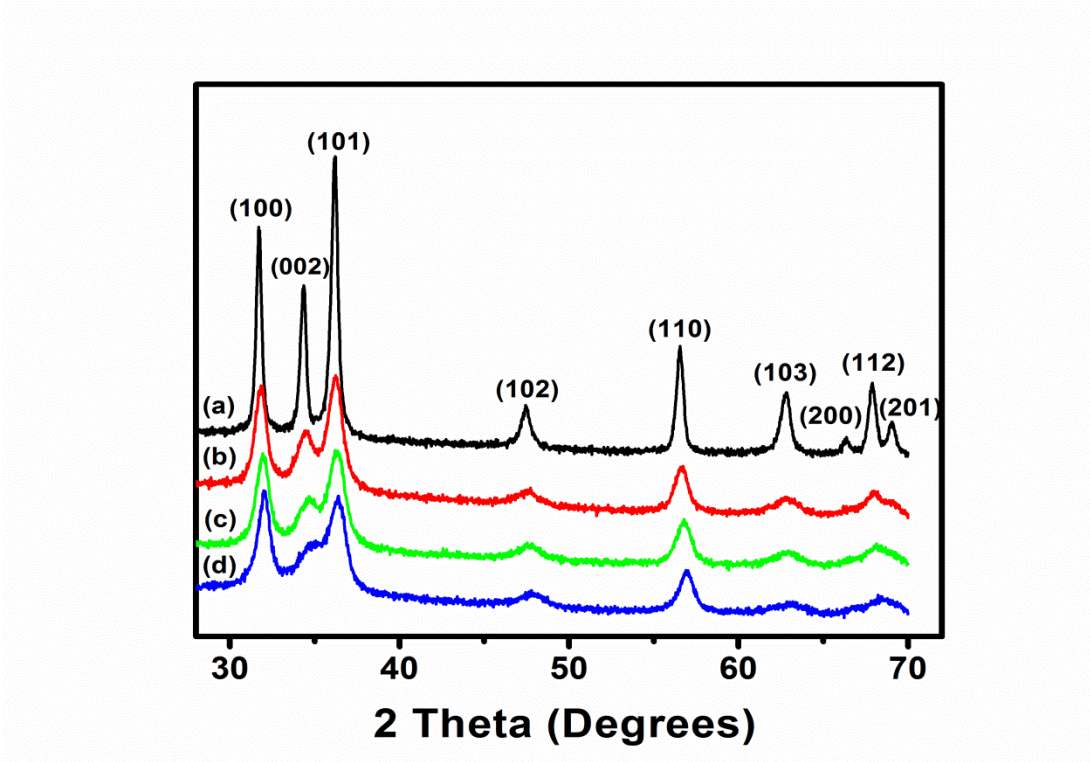

Figure 2. XRD spectra of (a) ZnO, (b) Al_2O_3/ZnO (5 wt%), (c) Al_2O_3/ZnO (10 wt%) and (d) Al_2O_3/ZnO (20 wt%) annealed nanotubes.

Table 4. Lattice constants and interplane distances of the prepared nanotubes

	a (nm)	**c (nm)**	**d (100)**	**d (002)**	**d (101)**
ZnO	0.325	0.521	0.282	0.261	0.248
Al_2O_3/ZnO (5 wt%)	0.324	0.519	0.281	0.260	0.247
Al_2O_3/ZnO (10 wt%)	0.323	0.517	0.280	0.258	0.246

Al_2O_3/ZnO (20 wt%)	0.322	0.516	0.279	0.258	0.245

3.2. Optical properties of ZnO and Al_2O_3/ZnO nanotubes

Reflectance spectra of ZnO and Al_2O_3/ZnO nanotubes samples are shown in Figure 3. A blue shift of the absorption edge of Al_2O_3/ZnO samples was found with the increase of Al_2O_3 doping concentration compared to ZnO nanotubes. Band gap energies of the samples were calculated from the reflectance spectra:[9]

$$(Fhv)^2 \sim (E_g - hv) \qquad \text{(Equation 8)}$$

where hv and E_g are the photon energy and the band gap, respectively. Parameter F, related to the absorption coefficient of the sample, was calculated as follow:[9]

$$F = (1- R)^2 / 2R \qquad \text{(Equation 9)}$$

where R is diffuse reflectance of the sample. The calculated band gap values are shown in Table 5. The increase of band gap of Al_2O_3/ZnO samples was observed with the increase of Al_2O_3 dopant amount. Previously, we have reported on optical properties of Al_2O_3/ZnO nanolaminates.[18] It was shown that Al_2O_3 sublayers changed the growth of ZnO nanolayers. Analysis of XRD and optical constants (refractive index and extinction coefficient) showed that Al_2O_3 do not dope ZnO during the growth. The blue shift of the band gap was supposedly due to the quantum confinement effect. In the present work, doping of ZnO with Al_2O_3 was proved by XRD data. The obtained grain size values are much higher than Bohr radius for ZnO (2.37 nm). Therefore, the blue shifted band gap value is due to Burstein-Moss effect.[19] The band gap of Al_2O_3/ZnO nanotubes (E_g) depends on the concentration of free electrons (n) as follow:[16]

$$E_g = E_{g0} + (h^2/8.m^*).(3/\pi)^{2/3}. n^{2/3} \qquad \text{(Equation 10)}$$

where, E_{g0}, h and m^* are the band gap of undoped ZnO nanotubes, the Plank's constant and the effective mass of electron, respectively. The obtained dependence of n vs Al_2O_3 dopant concentration is plotted in Figure 4. The concentration of free electrons linearly increased with Al_2O_3 doping. Therefore more electrons are available to take part in the photodegradation process compared to pure ZnO nanotubes. Urbach tail energy is an important parameter, which can assist the analysis of disorder in metal oxide nanostructure. It can be calculated from absorption spectrum using the following equation:[18]

$$F = F_0 \cdot e^{(hv-E_0)/E_u} \qquad \text{(Equation 11)}$$

F_0 and E_0 are specific parameters of the material; hv and E_u are the photon energy and Urbach energy, respectively. Parameter F was calculated using equation 7. The obtained E_u values are plotted in Figure 4. The increase of Al_2O_3 dopant concentration resulted in an increase of E_u, which can be related to the formation of defect states in the band gap of ZnO (Al^{3+} states, zinc interstitials, zinc vacancies …). From the obtained results, the photocatalytic activity under UV irradiation of Al_2O_3 doped ZnO is expected to be enhanced compared to pure ZnO nanotubes.

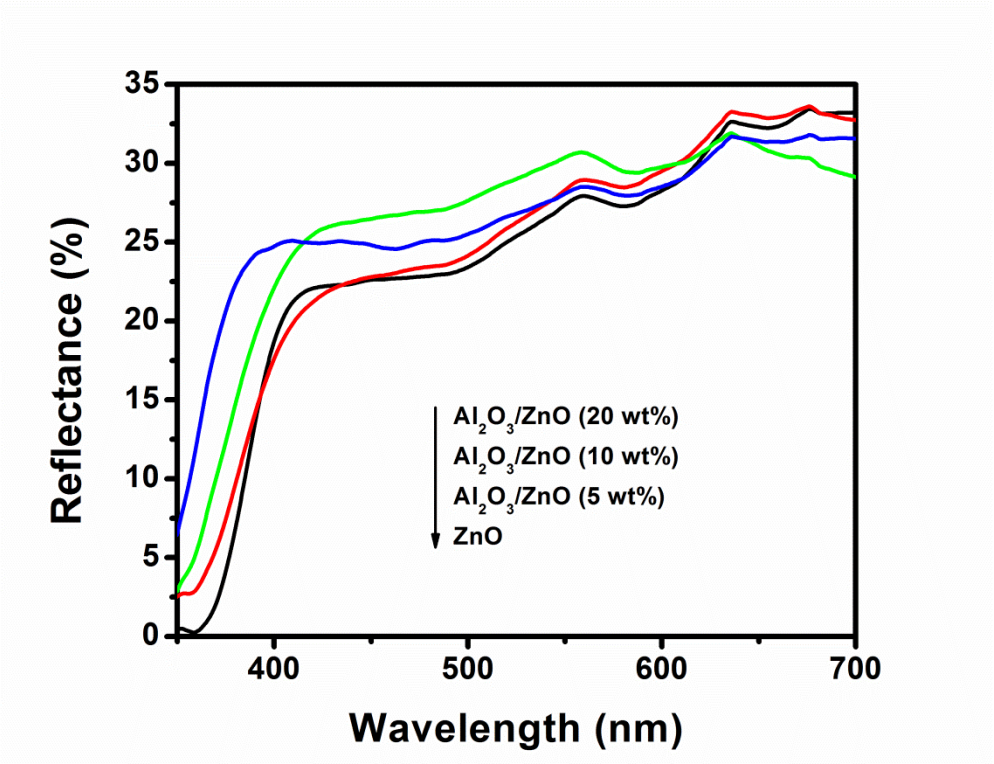

Figure 3. Reflectance spectra of ZnO, Al_2O_3/ZnO (5 wt%). Al_2O_3/ZnO (10 wt%) and Al_2O_3/ZnO (20 wt%) nanotubes.

Table 5. Band gap energies of ZnO and Al_2O_3/ZnO nanotubes.

Nanotubes	**ZnO**	**Al_2O_3/ZnO (5 wt%)**	**Al_2O_3/ZnO (10 wt%)**	**Al_2O_3/ZnO (20 wt%)**
E_g (eV)	3.18	3.24	3.31	3.42

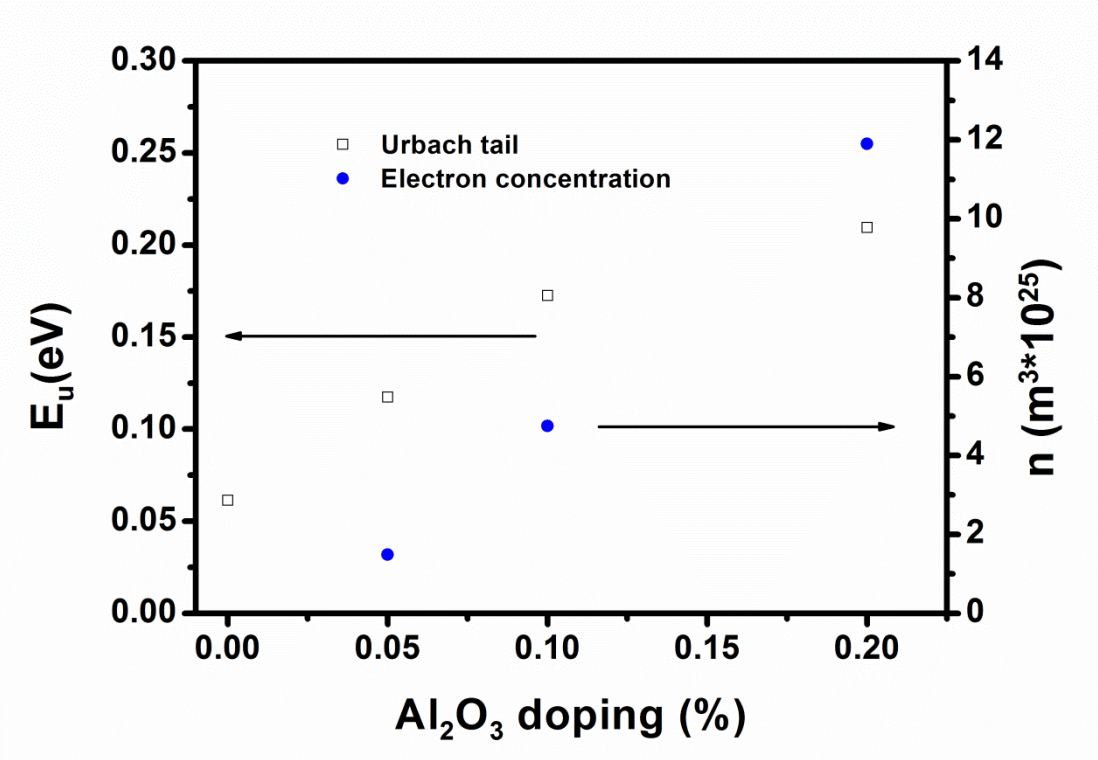

Figure 4. Evaluation of Urbach tail and free electron concentration with Al_2O_3 doping amounts.

Photoluminescence spectra of ZnO and Al_2O_3/ZnO nanotubes are shown in Figure 5. ZnO nanotubes showed PL spectrum with two emission bands in UV and Visible regions, centred at 385 and 570 nm, respectively. Al_2O_3 doped ZnO resulted in a change of the PL spectra. The wide emission bands were found at 420-440 nm and 490-560 nm for doped ZnO nanotubes with different concentration of Al_2O_3. Deconvolution of the PL spectra was performed with Gauss fitting using Origin software and the calculated peak positions are summarized in Table 6. For undoped ZnO, the PL peaks correspond to exciton emission (385 nm), shallow defects (406 nm), oxygen vacancies (502 and 550 nm) and oxygen interstitials (621 nm).[20] PL spectra of Al_2O_3/ZnO drastically depend on Al_2O_3 dopant concentration. At low doping concentration (5 wt%) a new peak related to Zn interstitials was observed at 416 nm. PL peaks in the range of 425-436 could correspond to Zn vacancies. PL peaks in the

range of 470-595 nm correspond to oxygen vacancies with different charge states (neutral, single and double ionized). PL peaks in the range of 630-710 nm correspond to donor-acceptor pairs, formed by Al^{3+} donor level and acceptor sites.[21, 22] As shown in Figure 5, PL spectra shift towards IR region when Al_2O_3 dopant amount increases. It was shown that Al_2O_3 dopant induced compressive strain and therefore defect formation. Oxygen vacancies are mostly formed within Al_2O_3 doping as discussed by Jule *et al.*[21] Therefore, IR shift of PL for highly doped ZnO is related to oxygen vacancies. Appearance of new peaks in the region of 634-710 could be due to the optical transitions between Al^{3+} donor sites and ionized oxygen vacancies.

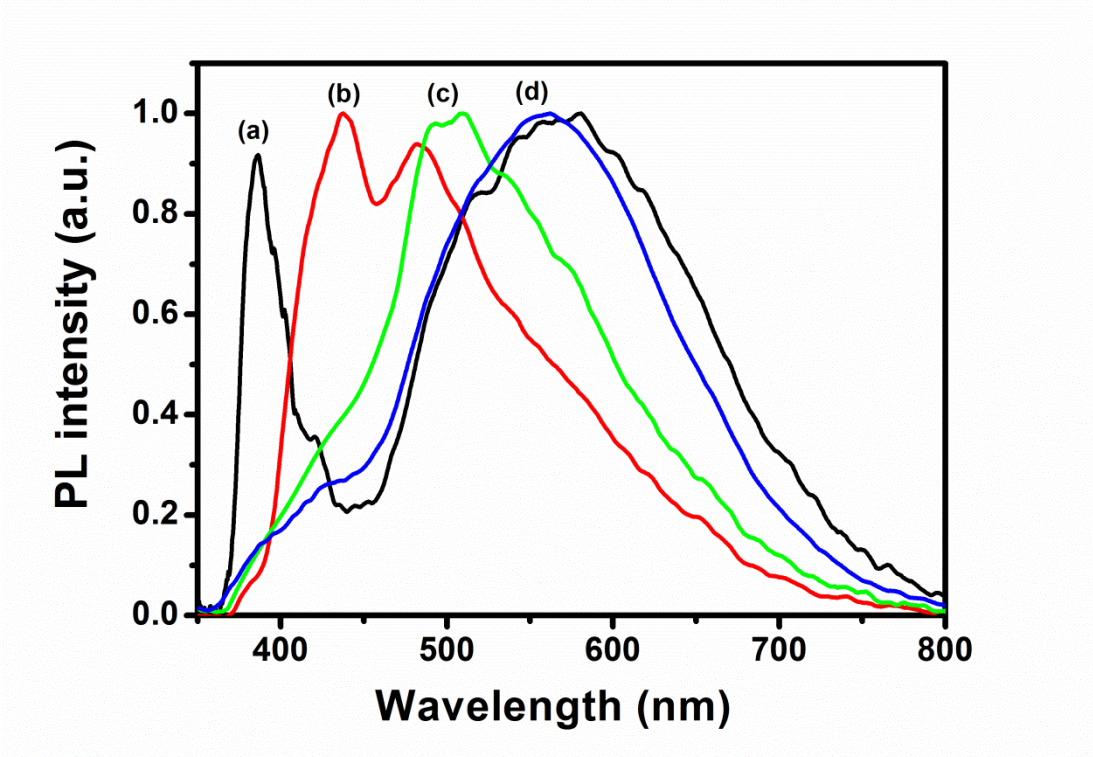

Figure 5. Photoluminescence spectra of (a) ZnO, (b) Al_2O_3/ZnO (5 wt%), (c)Al_2O_3/ZnO (10 wt%) and (d) Al_2O_3/ZnO (20 wt%) nanotubes.

Table 6. Peak positions of ZnO and Al_2O_3/ZnO nanotubes with different Al_2O_3 amounts.

	ZnO	Al_2O_3/ZnO (5 wt%)	Al_2O_3/ZnO (10 wt%)	Al_2O_3/ZnO (20 wt%)
Peak positions (nm)	385	416	434	425
	406	439	496	498
	502	475	536	546
	550	521	560	595
	621	604	634	653
	-	-	709	680

The infrared spectrum of Al_2O_3 doped ZnO with different amounts of Al_2O_3 in the range 400–3500 cm^{-1} are represented in Figure 6. The FTIR analysis allows us to observe two bands around 656 cm^{-1} and 715 cm^{-1}. The first one can be assigned to the Al-O stretching mode in octahedral structure and the second one corresponds to the tetrahedral Al-O bonds.[23] As we can note that the intensity of these bands is slightly increasing with Al_2O_3 amount deposited by ALD. Thus, the presence of Al_2O_3 phase in the prepared samples was detected as well by IR spectroscopy.

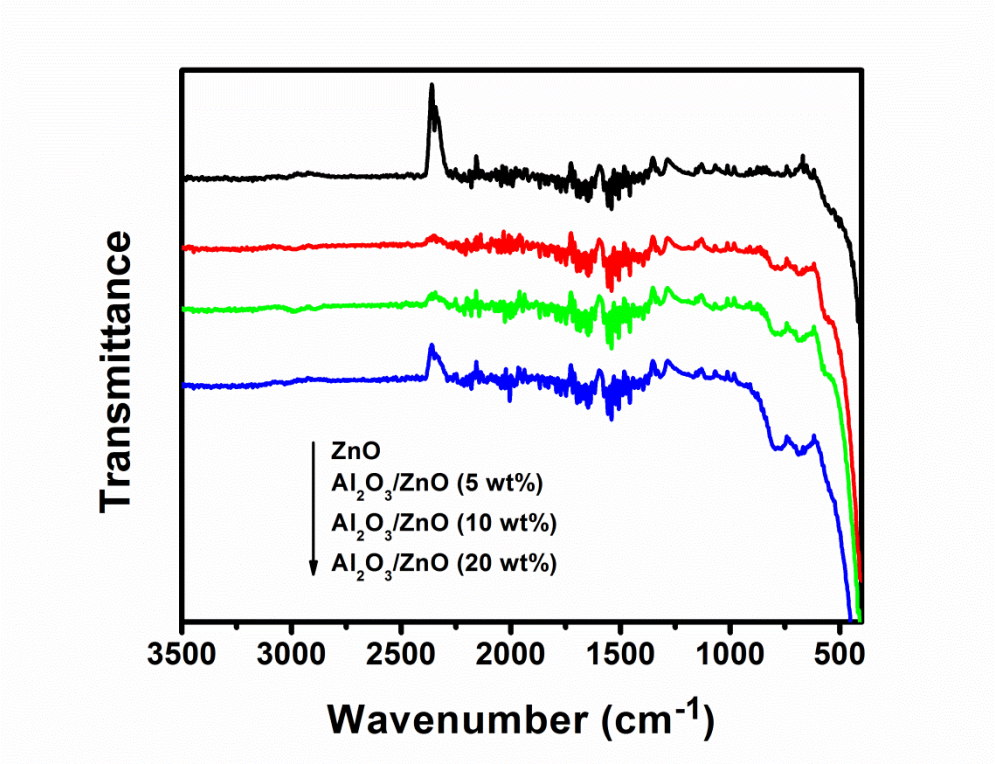

Figure 6. FTIR spectra of ZnO, Al_2O_3/ZnO (5 wt%). Al_2O_3/ZnO (10 wt%) and Al_2O_3/ZnO (20 wt%) nanotubes.

3.3. Photocatalytic activity

To evaluate the photodegradation efficiency of the as prepared samples under UV light (< 380 m), MO (major absorption band around 462 nm) was selected as model pollutant. Figure 7 shows the photodegradation curves of MB after 45 minutes with ZnO and Al_2O_3/ZnO nanotubes as catalysts. As results, it was found that in the absence of photocatalysts, MB was stable and difficult to be photodegraded under UV light. Under identical experimental conditions, the photodegradation percentages of MO were 57%, 80%, 89% and 98% in the presence of ZnO, Al_2O_3/ZnO (5 wt%), Al_2O_3/ZnO (10 wt%) and Al_2O_3/ZnO (20 wt%) nanotubes, respectively. As confirmed above by optical and structural analysis, the concentration of free electrons and the defects formation linearly increased with Al_2O_3 doping amount, thus the recombination of electron-hole pairs decreased. Therefore, the

photodegradation activity of Al_2O_3/ZnO under UV light is increased with Al_2O_3 doping concentration. As shown in Figure 8, the photocatalytic reactions follow a Langmuir–Hinshelwood first order kinetics model:[24]

$$r = dC/dt = kKC/(1+KC) \qquad \text{(Equation 12)}$$

where r, C, t, k and K are the degradation rate of MB (mg $(L\ min)^{-1}$), the concentration of the MB solution (mg L^{-1}), the irradiation time, the reaction rate constant (mg $(L\ min)^{-1}$), and the adsorption coefficient of MB (mg L^{-1}), respectively. The relationship between $\ln(C_0/C)$ and reaction time t is presented as follow:

$$\ln (C_0/C) = kKt = k_a t \quad \text{(Equation 13)}$$

where k_a and C are the apparent first-order rate constant (min^{-1}) and the concentration at time t, respectively. The k_a and R square value are reported in Table 7. The maximum rate constant (0.0884 min^{-1}) correspond to Al_2O_3/ZnO (20 wt%) sample which is 5, 3 and 2 times higher than that of pure ZnO, Al_2O_3/ZnO (5 wt%) and Al_2O_3/ZnO (10 wt%), respectively. Thus the Al_2O_3 doping effect improves the photocatalytic activity of ZnO under UV light.

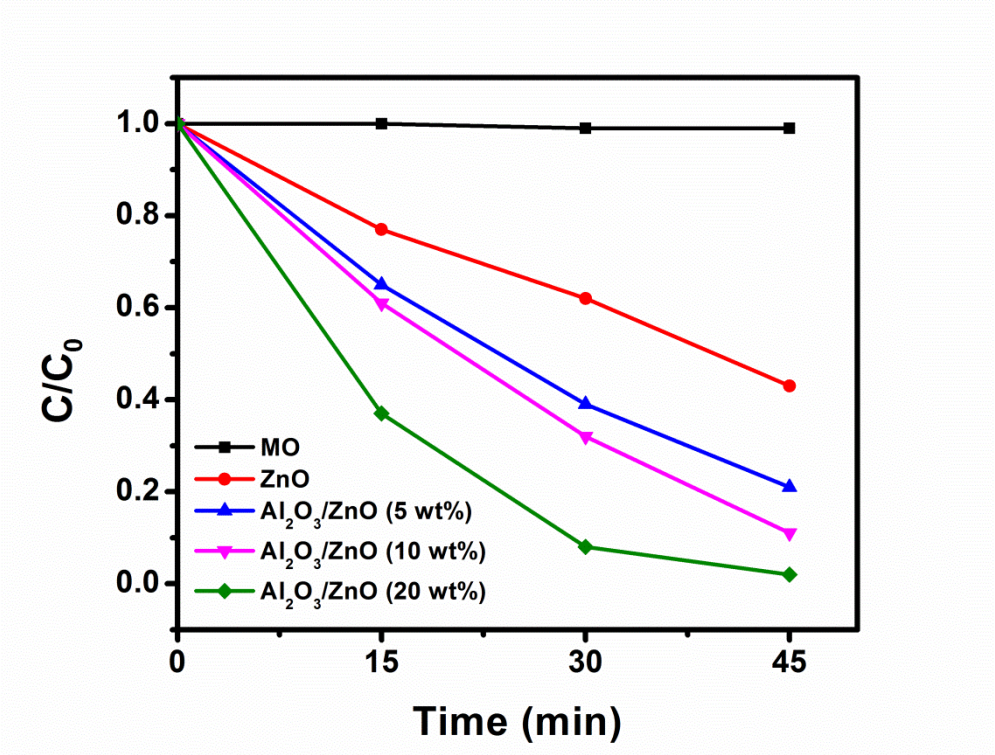

Figure 7. Photodegradation of MO by ZnO, Al_2O_3/ZnO (5 wt%). Al_2O_3/ZnO (10 wt%) and Al_2O_3/ZnO (20 wt%) photocatalysts under UV light.

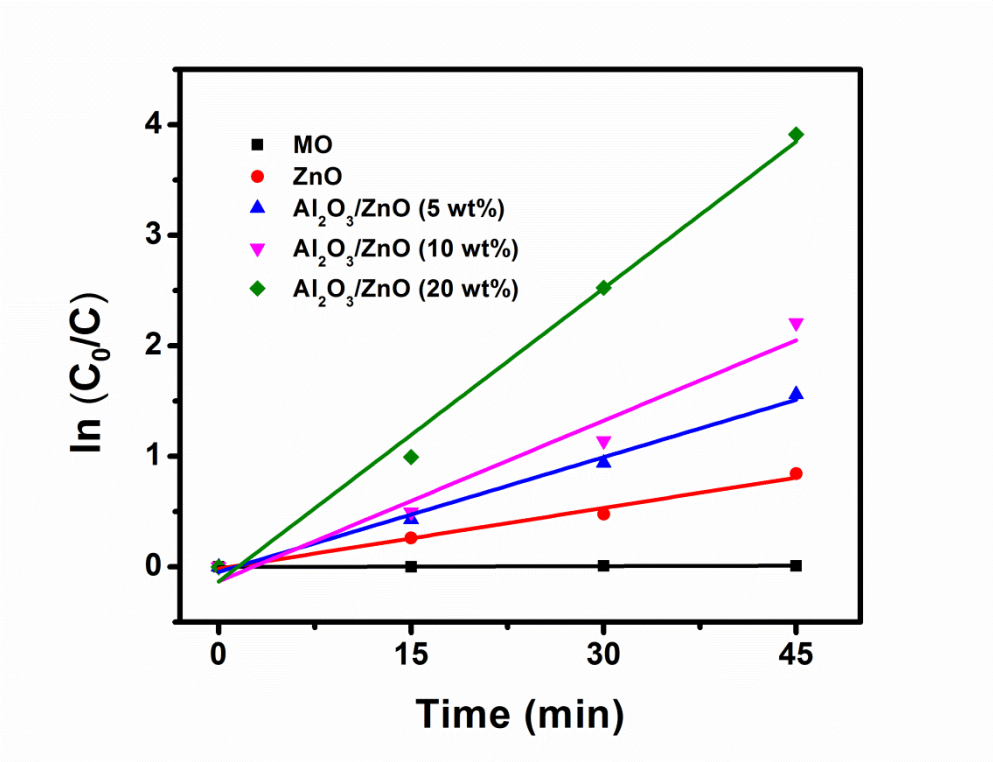

Figure 8. Kinetics of methyl orange degradation by the prepared samples.

Table 7. Kinetic parameters of ZnO and Al_2O_3/ZnO nanotubes.

	k_a (min^{-1})	**R^2**
MO	0.0002	0.9428
ZnO	0.0183	0.9819
Al_2O_3/ZnO (5 wt%)	0.0346	0.9901
Al_2O_3/ZnO (10 wt%)	0.0484	0.9527
Al_2O_3/ZnO (20 wt%)	0.0884	0.9895

Previous studies showed that the photocatalytic efficiency of the single-component semiconductor ZnO was seriously impeded due to its poor long term stability in photocatalysis.[25] Therefore in the present work the photocatalytic activity experiments of the prepared samples (ZnO, Al_2O_3/ZnO (5 wt%), Al_2O_3/ZnO (10 wt%) and Al_2O_3/ZnO (20 wt%) have been repeated for four cycles in order to investigate the potential reusability of these materials for the photocatalytic decomposition of MO solution under UV light irradiation. After each cycle, the catalyst was separated from the solution by centrifugation. From Figure 9, it can be seen that after 45 min of UV light irradiation and in the presence of the same photocatalysts, MO has been degraded in four repeated cycles. The slight decrease of efficiency for the Al_2O_3/ZnO nanotubes can be attributed to the loss of catalyst during centrifugation after each cycle. These results confirm that Al_2O_3/ZnO nanotubes with controlled ratio of Al_2O_3 have higher photodegradation efficiency and long-term stability in photocatalytic repeatability tests compared with pure ZnO nanotubes which have very low long-term photocatalytic stability.

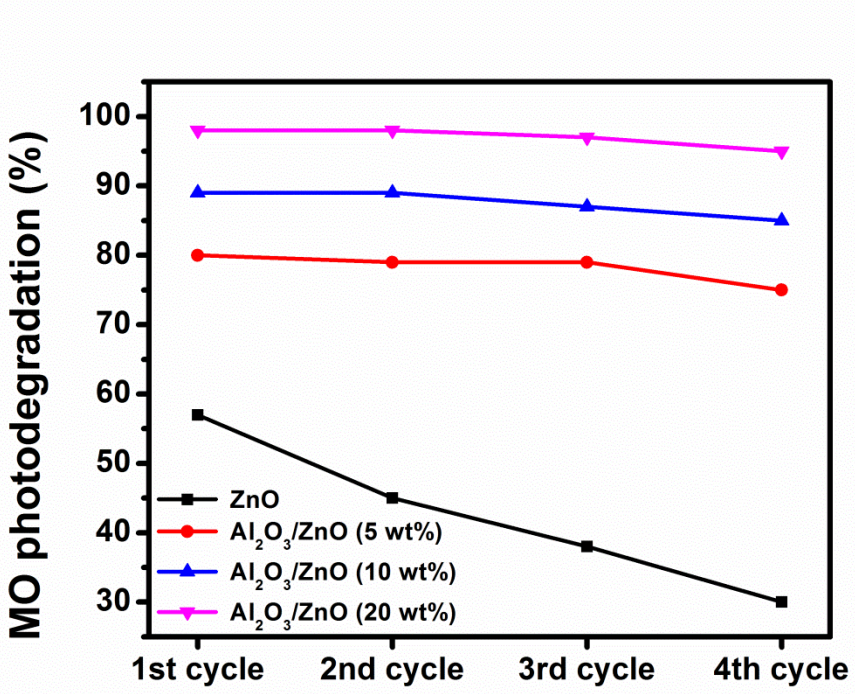

Figure 9 : Photocatalytic stability of ZnO, Al_2O_3/ZnO (5 wt%). Al_2O_3/ZnO (10 wt%) and Al_2O_3/ZnO (20 wt%) photocatalysts under UV light.

3. Conclusion

ZnO and Al_2O_3/ZnO nanotubes with controlled doping ratio of Al_2O_3 are successfully prepared by elecrospinning and atomic layer deposition techniques. All prepared samples were annealed at 500°C in air. After calcination, SEM images showed the nanotubes morphology of ZnO and Al_2O_3/ZnO samples. EDX data confirmed the increase of Al atomic percentage with the increasing of Al_2O_3 doping amount. The decrease of the crystalline structure due to the amorphous structure of Al_2O_3 and the increase of the strain values with Al_2O_3 doping concentration were detected from XRD data. The blue shift of Al_2O_3/ZnO band gap value due to the Burstein-Moss effect and the defect formation was confirmed by diffuse reflectance analysis. PL spectra analysis revealed that oxygen vacancies results in the IR shift of doped ZnO nanotubes. The photocatalytic degradation of methyl orange under UV light by Al_2O_3/ZnO (20 wt%) was 5 times higher than that of ZnO nanotubes. In conclusion, the defects formation and oxygen vacancies due to Al_2O_3 doping increase the charge separation efficiency of ZnO, thus enhancing the stability of its photoactivity under UV light. Therefore, the photocatalytic activity is greatly depending on the optical and structural properties of the material. The ability to tune the optical and structural properties of our synthesized materials could be promising in different applications such as the production of optical sensors and biosensors.[26-29]

Acknowledgements. M. Nasr would like to thank the Lebanese University for the PhD funding. This study was partially supported by the ANR project ANR-14-CE07-0011 “BONALD”.

List of Figures

References

[1] J. Elias, I. Utke, S. Yoon, M. Bechelany, A. Weidenkaff, J. Michler, L. Philippe, Electrochemical growth of ZnO nanowires on atomic layer deposition coated polystyrene sphere templates, Electrochimica Acta, 110 (2013) 387-392.

[2] J. Chen, F. Qiu, W. Xu, S. Cao, H. Zhu, Recent progress in enhancing photocatalytic efficiency of TiO_2-based materials, Applied Catalysis A: General, 495 (2015) 131-140.

[3] M. Bechelany, A. Amin, A. Brioude, D. Cornu, P. Miele, ZnO nanotubes by template-assisted sol–gel route, Journal of Nanoparticle Research, 14 (2012) 980.

[4] R. Georgekutty, M.K. Seery, S.C. Pillai, A highly efficient Ag-ZnO photocatalyst: synthesis, properties, and mechanism, The Journal of Physical Chemistry C, 112 (2008) 13563-13570.

[5] L. Zheng, Y. Zheng, C. Chen, Y. Zhan, X. Lin, Q. Zheng, K. Wei, J. Zhu, Network structured SnO_2/ZnO heterojunction nanocatalyst with high photocatalytic activity, Inorganic Chemistry, 48 (2009) 1819-1825.

[6] Z. Wang, B. Huang, Y. Dai, X. Qin, X. Zhang, P. Wang, H. Liu, J. Yu, Highly photocatalytic ZnO/In_2O_3 heteronanostructures synthesized by a coprecipitation method, The Journal of Physical Chemistry C, 113 (2009) 4612-4617.

[7] A. Hameed, T. Montini, V. Gombac, P. Fornasiero, Photocatalytic decolourization of dyes on NiO–ZnO nano-composites, Photochemical & Photobiological Sciences, 8 (2009) 677-682.

[8] R. Viter, I. Iatsunskyi, V. Fedorenko, S. Tumenas, Z. Balevicius, A. Ramanavicius, S. Balme, M. Kempiński, G. Nowaczyk, S. Jurga, Enhancement of electronic and optical properties of ZnO/Al_2O_3 nanolaminate coated electrospun nanofibers, The Journal of Physical Chemistry C, 120 (2016) 5124-5132.

[9] M. Baitimirova, R. Viter, J. Andzane, A. van der Lee, D. Voiry, I. Iatsunskyi, E. Coy, L. Mikoliunaite, S. Tumenas, K. Załęski, Tuning of Structural and Optical Properties of Graphene/ZnO Nanolaminates, The Journal of Physical Chemistry C, 120 (2016) 23716-23725.

[10] M. Nasr, A.A. Chaaya, N. Abboud, M. Bechelany, R. Viter, C. Eid, A. Khoury, P. Miele, Photoluminescence: A very sensitive tool to detect the presence of anatase in rutile phase electrospun TiO_2 nanofibers, Superlattices and Microstructures, 77 (2015) 18-24.

[11] D. Selloum, A.A. Chaaya, M. Bechelany, V. Rouessac, P. Miele, S. Tingry, A highly efficient gold/electrospun PAN fiber material for improved laccase biocathodes for biofuel cell applications, Journal of Materials Chemistry A, 2 (2014) 2794-2800.

[12] S. Cabello-Aguilar, S. Balme, A.A. Chaaya, M. Bechelany, E. Balanzat, J.-M. Janot, C. Pochat-Bohatier, P. Miele, P. Dejardin, Slow translocation of polynucleotides and their discrimination by α-hemolysin inside a single track-etched nanopore designed by atomic layer deposition, Nanoscale, 5 (2013) 9582-9586.

[13] I.K. Konstantinou, T.A. Albanis, TiO_2-assisted photocatalytic degradation of azo dyes in aqueous solution: kinetic and mechanistic investigations: a review, Applied Catalysis B: Environmental, 49 (2004) 1-14.

[14] A.L. Linsebigler, G. Lu, J.T. Yates Jr, Photocatalysis on TiO_2 surfaces: principles, mechanisms, and selected results, Chemical reviews, 95 (1995) 735-758.

[15] M. Nasr, R. Viter, C. Eid, F. Warmont, R. Habchi, P. Miele, M. Bechelany, Synthesis of novel $ZnO/ZnAl_2O_4$ multi co-centric nanotubes and their long-term stability in photocatalytic application, RSC Advances, 6 (2016) 103692-103699.

[16] C.-H. Zhai, R.-J. Zhang, X. Chen, Y.-X. Zheng, S.-Y. Wang, J. Liu, N. Dai, L.-Y. Chen, Effects of Al Doping on the Properties of ZnO Thin Films Deposited by Atomic Layer Deposition, Nanoscale Research Letters, 11 (2016) 407.

[17] M. Nasr, R. Viter, C. Eid, R. Habchi, P. Miele, M. Bechelany, Enhanced photocatalytic performance of novel electrospun BN/TiO 2 composite nanofibers, New Journal of Chemistry, 41 (2017) 81-89.

[18] A.A. Chaaya, R. Viter, I. Baleviciute, M. Bechelany, A. Ramanavicius, Z. Gertnere, D. Erts, V. Smyntyna, P. Miele, Tuning optical properties of Al_2O_3/ZnO nanolaminates synthesized by atomic layer deposition, The Journal of Physical Chemistry C, 118 (2014) 3811-3819.

[19] A.A. Chaaya, R. Viter, I. Baleviciute, M. Bechelany, A. Ramanavicius, D. Erts, V. Smyntyna, P. Miele, Optical and structural properties of Al_2O_3/ZnO nanolaminates deposited by ALD method, Physica status solidi (c), 11 (2014) 1505-1508.

[20] A.A. Chaaya, R. Viter, M. Bechelany, Z. Alute, D. Erts, A. Zalesskaya, K. Kovalevskis, V. Rouessac, V. Smyntyna, P. Miele, Evolution of microstructure and related optical properties of ZnO grown by atomic layer deposition, Beilstein journal of nanotechnology, 4 (2013) 690-698.

[21] L. Jule, F. Dejene, A.G. Ali, K. Roro, B. Mwakikunga, Defect-induced room temperature ferromagnetic properties of the Al-doped and undoped ZnO rod-like nanostructure, Materials Letters, DOI (2017).

[22] K. Sandeep, S. Bhat, S. Dharmaprakash, Structural, optical, and LED characteristics of ZnO and Al doped ZnO thin films, Journal of Physics and Chemistry of Solids, DOI (2017).

[23] K. Djebaili, Z. Mekhalif, A. Boumaza, A. Djelloul, XPS, FTIR, EDX, and XRD analysis of Al_2O_3 scales grown on PM2000 alloy, Journal of Spectroscopy, 2015 (2015).

[24] M. Nasr, S. Balme, C. Eid, R. Habchi, P. Miele, M. Bechelany, Enhanced Visible-Light Photocatalytic Performance of Electrospun rGO/TiO_2 Composite Nanofibers, The Journal of Physical Chemistry C, DOI (2016).

[25] J.K. Kim, S. Bae, W. Kim, M.J. Jeong, S.H. Lee, C.-L. Lee, W.K. Choi, J.Y. Hwang, J.H. Park, D.I. Son, Nano carbon conformal coating strategy for enhanced photoelectrochemical responses and long-term stability of ZnO quantum dots, Nano Energy, 13 (2015) 258-266.

[26] A. Tereshchenko, M. Bechelany, R. Viter, V. Khranovskyy, V. Smyntyna, N. Starodub, R. Yakimova, Optical biosensors based on ZnO nanostructures: advantages and perspectives. A review, Sensors and Actuators B: Chemical, 229 (2016) 664-677.

[27] A. Tereshchenko, V. Fedorenko, V. Smyntyna, I. Konup, A. Konup, M. Eriksson, R. Yakimova, A. Ramanavicius, S. Balme, M. Bechelany, ZnO films formed by atomic layer deposition as an optical biosensor platform for the detection of Grapevine virus A-type proteins, Biosensors and Bioelectronics, DOI (2016).

[28] A. Choi, K. Kim, H.-I. Jung, S.Y. Lee, ZnO nanowire biosensors for detection of biomolecular interactions in enhancement mode, Sensors and Actuators B: Chemical, 148 (2010) 577-582.

[29] A.G. Joshi, S. Sahai, N. Gandhi, Y.R. Krishna, D. Haranath, Valence band and core-level analysis of highly luminescent ZnO nanocrystals for designing ultrafast optical sensors, Applied Physics Letters, 96 (2010) 123102.